



OPEN

CONFERENCE  
PROCEEDINGS

APEnergy2014

.....

SUBJECT AREAS:

BATTERIES

CHEMICAL ENGINEERING

SYNTHESIS AND PROCESSING

Received

27 February 2014

Accepted

18 June 2014

Published

29 August 2014

Correspondence and  
requests for materials  
should be addressed to  
Y.C.K. (yckang@  
konkuk.ac.kr)

# Electrochemical properties of tungsten sulfide–carbon composite microspheres prepared by spray pyrolysis

Seung Ho Choi<sup>1</sup>, Sung Jin Boo<sup>1</sup>, Jong-Heun Lee<sup>2</sup> & Yun Chan Kang<sup>1</sup>

<sup>1</sup>Department of Chemical Engineering, Konkuk University, 1 Hwayang-dong, Gwangjin-gu, Seoul 143-701, Republic of Korea, <sup>2</sup>Department of Materials Science and Engineering, Korea University, Anam-Dong, Seongbuk-Gu, Seoul 136-713, Republic of Korea.

Tungsten sulfide (WS<sub>2</sub>)–carbon composite powders with superior electrochemical properties are prepared by a two-step process. WO<sub>3</sub>–carbon composite powders were first prepared by conventional spray pyrolysis, and they were then sulfidated to form WS<sub>2</sub>–carbon powders. Bare WS<sub>2</sub> powders are also prepared by sulfidation of bare WO<sub>3</sub> powders obtained by spray pyrolysis. Stacked graphitic layers could not be found in the bare WS<sub>2</sub> and WS<sub>2</sub>–carbon composite powders. The amorphous bare WS<sub>2</sub> and WS<sub>2</sub>–carbon composite powders have Brunauer–Emmett–Teller (BET) surface areas of 2.8 and 4 m<sup>2</sup> g<sup>-1</sup>, respectively. The initial discharge and charge capacities of the WS<sub>2</sub>–carbon composite powders at a current density of 100 mA g<sup>-1</sup> are 1055 and 714 mA h g<sup>-1</sup>, respectively, and the corresponding initial Coulombic efficiency is 68%. On the other hand, the initial discharge and charge capacities of the bare WS<sub>2</sub> powders are 514 and 346 mA h g<sup>-1</sup>, respectively. The discharge capacities of the WS<sub>2</sub>–carbon composite powders for the 2<sup>nd</sup> and 50<sup>th</sup> cycles are 716 and 555 mA h g<sup>-1</sup>, respectively, and the corresponding capacity retention measured after first cycle is 78%.

Transition metal sulfides (M<sub>x</sub>S<sub>y</sub>, M = W, Mo, Zn, Mn, Ni, Fe) with various morphologies prepared by conventional liquid solution processes have been investigated as promising anode materials for lithium-ion batteries (LIBs)<sup>1,2</sup>. In particular, layered dichalcogenide materials (MoS<sub>2</sub> and WS<sub>2</sub>), which have van der Waals forces across the gaps between the S–M–S sheets, thus allowing the Li ions to diffuse without a significant increase in volume expansion, have higher structural stabilities during repeated lithiation and delithiation processes as compared with transition metal oxides and tin oxide studied widely as anode materials for LIBs<sup>3–19</sup>. In addition, transition metal dichalcogenides have better electronic and ionic conductivities than transition metal oxides and tin oxide. However, the electronic conductivity of transition metal dichalcogenides is still lower as compared to carbon-based materials<sup>15</sup>. Carbonaceous materials, including graphene, carbon nanotubes, and amorphous carbon, have been composited with transition metal dichalcogenides in order to improve their electrochemical properties<sup>5–17</sup>. Various structured MoS<sub>2</sub>–carbon composite materials prepared by liquid solution methods have been studied as anode materials for LIBs<sup>5–13</sup>. However, the preparation of WS<sub>2</sub>–carbon composite materials and their electrochemical properties have been scarcely studied<sup>4–17</sup>. WS<sub>2</sub>–graphene composite materials had better cycling and rate performances than bare WS<sub>2</sub> powders<sup>15</sup>.

Commercial LIB anode materials typically comprise spherical powders with sizes of several microns. However, micron-sized metal sulfide–carbon composite powders with spherical particles and superior electrochemical properties have been scarcely studied in the conventional liquid solution processes. In this study, tungsten sulfide (WS<sub>2</sub>)–carbon composite powders with superior electrochemical properties were prepared by a two-step process. WO<sub>3</sub>–carbon composite powders prepared by spray pyrolysis (Figure S1) were sulfidated to form the WS<sub>2</sub>–carbon composite powders<sup>20,21</sup>. The spherical shape and micron size of the WO<sub>3</sub>–carbon composite powders were maintained even after the sulfidation process. The electrochemical properties of the WS<sub>2</sub>–carbon composite powders were compared to those of the bare WS<sub>2</sub> powders. The WS<sub>2</sub>–carbon composite powders had higher capacities than the bare WS<sub>2</sub> powders.

## Results

The WO<sub>3</sub> and WO<sub>3</sub>–carbon composite powders prepared by spray pyrolysis were transformed into WS<sub>2</sub> and WS<sub>2</sub>–carbon composite powders, respectively, by a sulfidation process. The morphologies and crystal structures

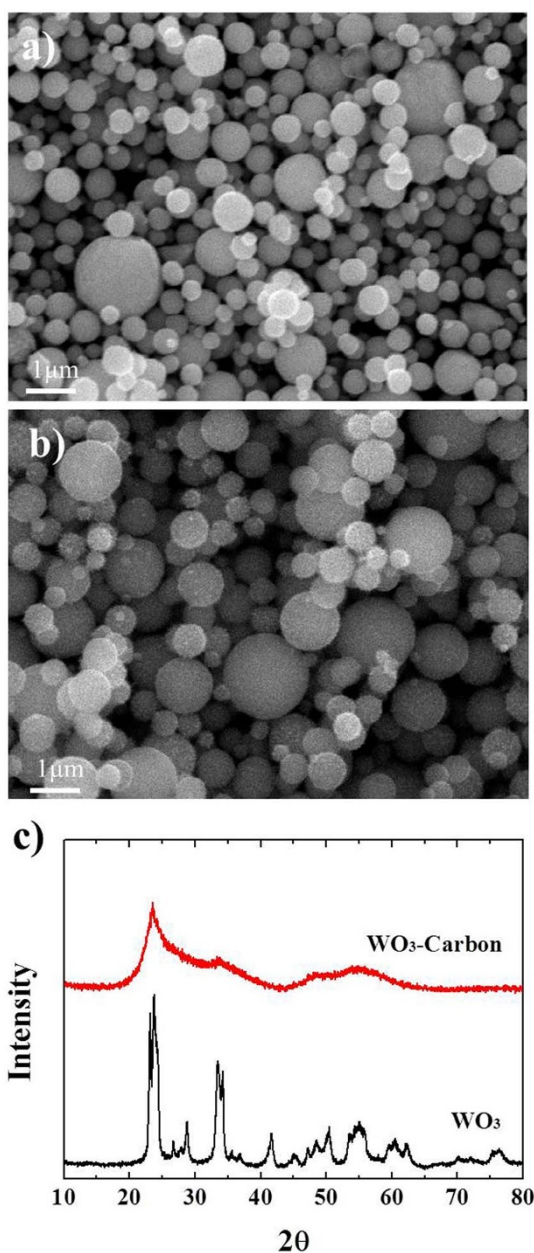


**Figure 1** | Morphologies and crystal structures of the bare  $\text{WO}_3$  and  $\text{WO}_3$ -carbon composite powders: (a) SEM image of bare  $\text{WO}_3$ , (b) SEM image of  $\text{WO}_3$ -carbon, and (c) XRD patterns.

of the bare  $\text{WO}_3$  and  $\text{WO}_3$ -carbon composite powders prepared by spray pyrolysis under nitrogen atmosphere are shown in Figure 1. The carbon component was formed by polymerization and the carbonization of sucrose dissolved into the spray solution. The powders had a spherical shape and nonaggregation characteristics, regardless of the carbon component. One particle with spherical shape was formed from one droplet by gas phase reaction. The  $\text{WO}_3$ -carbon composite powders with high carbon content had a larger mean size than the bare  $\text{WO}_3$  powders, as shown in the SEM images in Figures 1a and 1b. The bare  $\text{WO}_3$  powders had a sharp monoclinic crystal structure without impurity peaks as shown in Figure 1c. On the other hand, the  $\text{WO}_3$ -carbon composite powders had an amorphous structure with low-intensity crystalline peaks.

Figure 2a shows the XRD patterns of the sulfidated powders. The  $\text{WS}_2$  and  $\text{WS}_2$ -carbon composite powders had pure crystal structures of a hexagonal  $\text{WS}_2$  phase without impurity peaks of  $\text{WO}_3$ , even though the two samples had different crystal orientations. The (002)

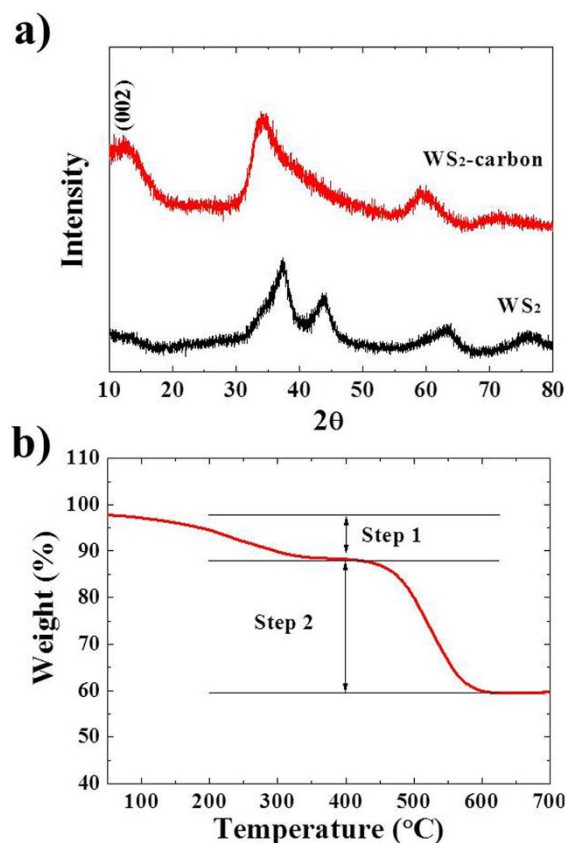


**Figure 2** | (a) XRD patterns of the bare  $\text{WS}_2$  and  $\text{WS}_2$ -carbon composite and (b) TG curve of the  $\text{WS}_2$ -carbon composite.

reflection indicating stacking of the  $\text{WS}_2$  layers was only observed in the  $\text{WS}_2$ -carbon composite powders. The XRD patterns had broad peaks with low intensities. The amorphous  $\text{WS}_2$  and  $\text{WS}_2$ -carbon composite powders were prepared because of a low sulfidation temperature of  $400^\circ\text{C}$ . Figure 2b shows the thermogravimetry (TG) curve of the  $\text{WS}_2$ -carbon composite powders. The TG curve had two distinct weight losses below  $700^\circ\text{C}$ . The weight loss by complete oxidation of  $\text{WS}_2$  into  $\text{WO}_3$  under air atmosphere was as low as 6.5 wt%. Therefore, the two-step weight losses observed near 200 and  $400^\circ\text{C}$  were mainly due to the decomposition of carbon components. The composition of the  $\text{WS}_2$ -carbon composite powders with a dense structure occurred in two steps. The calculated carbon content of the  $\text{WS}_2$ -carbon composite powders calculated from the TG results was about 30 wt%.

The morphologies of the  $\text{WS}_2$ -carbon composite powders are shown in Figure 3. The composite powders had morphology similar to that of the  $\text{WO}_3$ -carbon composite powders, indicating that the sulfidation process did not significantly change the morphology of the powders. The high-resolution TEM images shown in Figures 3c and 3d reveal slightly crystalline  $\text{WS}_2$  that consists of a few graphitic layers near the surface of the powder. The interlayer distance of the (002) plane measured from the TEM image is 0.63 nm<sup>14</sup>. However, the stacked graphitic layers were not found in the inner part of the composite powders, as shown by the dotted rectangular in Figure 3d. The dot-mapping images shown in Figure 3e show the uniform distributions of the W, S, and C components all over the  $\text{WS}_2$ -carbon composite powder. Complete sulfidation of the powders occurred. The uniform distribution of carbon all over the powders disturbed the growth of  $\text{WS}_2$  crystals. Figure 4 shows the morphologies of the bare  $\text{WS}_2$  powders. The bare  $\text{WS}_2$  powders also had a spherical shape like the  $\text{WS}_2$ -carbon composite powders. The high-resolution TEM images shown in Figures 4c and 4d show the non-stacked  $\text{WS}_2$  layers

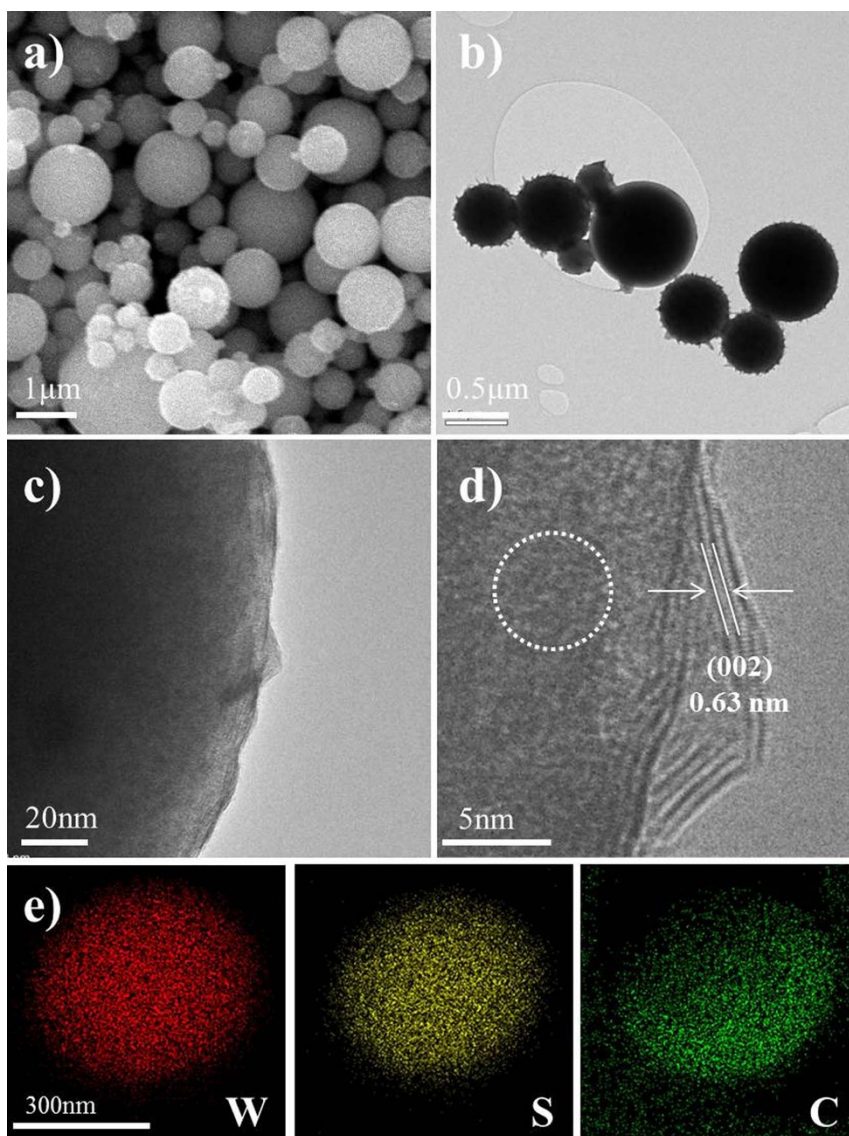


**Figure 3** | Morphologies of the WS<sub>2</sub>-carbon composite powders: (a) SEM image, (b) low resolution TEM image, (c) and (d) high resolution TEM images, and (e) dot-mapping images.

and amorphous structure, respectively. The bare WS<sub>2</sub> and WS<sub>2</sub>-carbon composite powders had Brunauer–Emmett–Teller (BET) surface areas of 2.8 and 4 m<sup>2</sup> g<sup>-1</sup>, respectively. The dense structures of the WS<sub>2</sub> and WS<sub>2</sub>-carbon composite powders without pores, as shown by the TEM images in Figures 3 and 4, resulted in low BET surface areas.

The electrochemical properties of the bare WS<sub>2</sub> and WS<sub>2</sub>-carbon composite powders are shown in Figure 5. Figure 5a shows the cyclic voltammograms (CVs) of the WS<sub>2</sub>-carbon composite powders measured at a scan rate of 0.4 mV s<sup>-1</sup> in the voltage range of 0.001–3 V. The first discharge curve had two broad reduction peaks near 0.5 and 0.1 V. The mesoporous WS<sub>2</sub> powders with high crystallinity prepared by a vacuum assisted impregnation route had sharp reduction and oxidation peaks in their CV curves<sup>14</sup>. However, the amorphous WS<sub>2</sub>-carbon composite powders had broad reduction and oxidation peaks in all cycles. The clear reduction peaks for the lithium insertion to WS<sub>2</sub> to form Li<sub>x</sub>WS<sub>2</sub> (WS<sub>2</sub> + xLi<sup>+</sup> + xe<sup>-</sup> => Li<sub>x</sub>WS<sub>2</sub>) and the conversion reaction (WS<sub>2</sub> + 4Li<sup>+</sup> + 4e<sup>-</sup> => W + 2Li<sub>2</sub>S) were not observed<sup>15</sup>. The steady CV profiles after the initial cycle indicated high stability and reversibility of the WS<sub>2</sub>-carbon composite powders for Li<sup>+</sup> insertion and extraction. Figure 5b shows the charge and discharge curves of the WS<sub>2</sub>-carbon composite powders at a con-

stant current density of 100 mA g<sup>-1</sup>. The charge and discharge curves for all cycles, including the first cycle, had no distinct plateaus. These results well coincide with those of the CVs shown in Figure 5a. The cycle curves of the bare WS<sub>2</sub> powders with amorphous structure shown in Figure S2 also had no distinct plateaus. The initial discharge and charge capacities of the WS<sub>2</sub>-carbon composite powders were 1055 and 714 mA h g<sup>-1</sup>, respectively, and the corresponding initial Coulombic efficiency was 68%. On the other hand, the initial discharge and charge capacities of the bare WS<sub>2</sub> powders were 514 and 346 mA h g<sup>-1</sup>, respectively, and the corresponding initial Coulombic efficiency was 67%. The rate performance of the WS<sub>2</sub>-carbon composite powders is shown in Figure S3, wherein the current density increased stepwise from 50 to 500 mA g<sup>-1</sup>, and then returned to 50 mA g<sup>-1</sup>. The WS<sub>2</sub>-carbon composite powders exhibited the final discharge capacities of 761, 630, 561, 524, and 502 mA h g<sup>-1</sup> at current densities of 50, 150, 300, 400, and 500 mA g<sup>-1</sup>, respectively. When the current density returned to 50 mA g<sup>-1</sup>, the discharge capacity recovered to 678 mA h g<sup>-1</sup>.

## Discussion

Electrochemical impedance spectroscopy was conducted to determine the Li<sup>+</sup> ion transfer behavior in the bare WS<sub>2</sub> and WS<sub>2</sub>-carbon

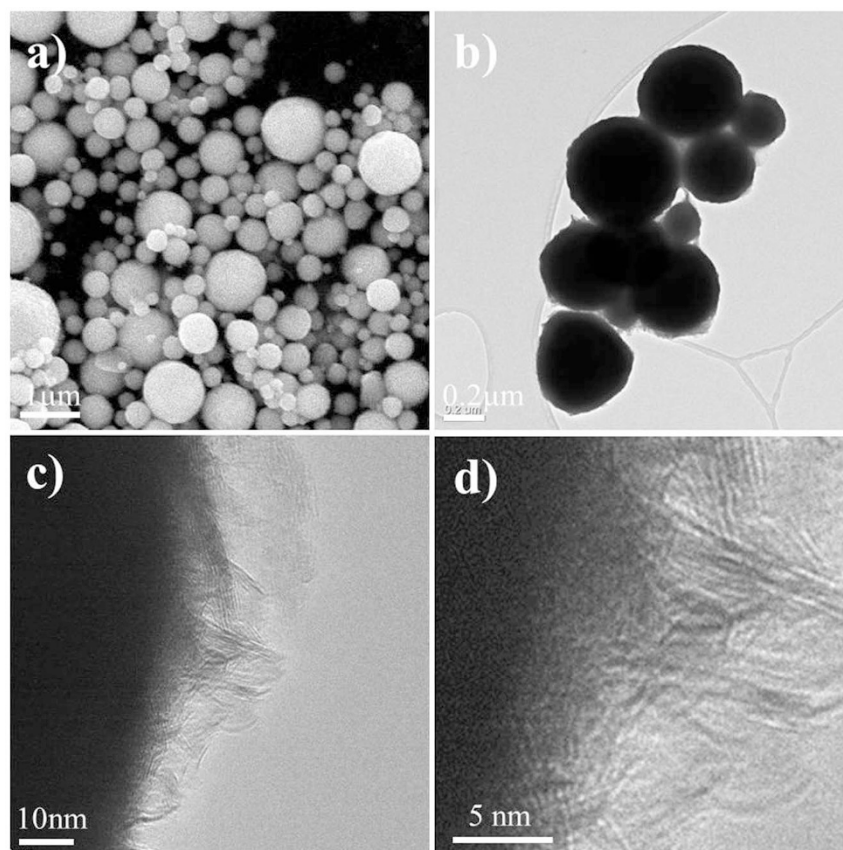


**Figure 4** | Morphologies of the bare WS<sub>2</sub> powders: (a) SEM image, (b) low resolution TEM image, (c) and (d) high resolution TEM images.

composite powders. The Nyquist impedance plots obtained before cycling are shown in Figure 5c. The semicircular diameter, which shows the charge-transfer resistance ( $R_{ct}$ ) obtained in the medium-frequency region for the WS<sub>2</sub>-carbon composite powders, was similar to that in the case of the bare WS<sub>2</sub> powders. Generally, the high BET surface area increased the  $R_{ct}$  of the powders. However, the high conductivity decreased the  $R_{ct}$  of the WS<sub>2</sub>-carbon composite powders. The relationship between the real part of the impedance ( $Z_{re}$ ) and  $\omega^{-1/2}$  (where  $\omega$  is the angular frequency in the low-frequency region,  $\omega = 2\pi f$ ) in the low-frequency region is shown in the Figure S4<sup>22,23</sup>. The low slope ( $\sigma$ , Warburg impedance coefficient) of  $Z_{re}$  versus  $\omega^{-1/2}$  revealed the high lithium ion diffusion rate of the WS<sub>2</sub>-carbon composite powders. Figure 5d shows the cycling performances of the bare WS<sub>2</sub> and WS<sub>2</sub>-carbon composite powders at a current density of 100 mA g<sup>-1</sup>. The discharge capacities of the WS<sub>2</sub>-carbon composite powders for the 2<sup>nd</sup> and 50<sup>th</sup> cycles were 716 and 555 mA h g<sup>-1</sup>, respectively, and the corresponding capacity retention measured after the first cycle was 78%. On the other hand, the discharge capacities of the bare WS<sub>2</sub> powders for the 2<sup>nd</sup> and 50<sup>th</sup> cycles were 356 and 304 mA h g<sup>-1</sup>, respectively, and the corresponding capacity retention measured after the first cycle was 85%. The bare WS<sub>2</sub> powders had good cycling performance even though they had low initial discharge and charge capacities. Figure S5 shows the morphologies and EDS spectra of the bare WS<sub>2</sub> and WS<sub>2</sub>-carbon composite powders after 50 cycles. The two samples maintained their spherical morphologies even after cycling as shown by SEM images. The high structural stabilities of the powders improved their cycling performances. However, the TEM images showed the different structures of the bare WS<sub>2</sub> and WS<sub>2</sub>-carbon composite powders after cycling. The thick layer owing to the formation of a polymeric gel-like film during cycling covered the bare WS<sub>2</sub> material. The main component of the layer covering the bare WS<sub>2</sub> powder observed by EDS spectrum was carbon.

Phase-pure WS<sub>2</sub>-carbon composite powders with uniform distribution of W, S, and C components were prepared by applying ultrasonic spray pyrolysis. The WS<sub>2</sub>-carbon composite powders had a spherical shape, dense structure, and amorphous crystal structure. Amorphous WO<sub>3</sub>-carbon composite powders with high carbon content were transformed into amorphous WS<sub>2</sub>-carbon composite powders. However, highly crystalline bare WO<sub>3</sub> powders prepared by spray pyrolysis were transformed into amorphous bare WS<sub>2</sub> powders by a sulfidation process. The cyclic voltammograms and initial discharge and charge curves revealed the amorphous structure of the WS<sub>2</sub>-carbon composite powders. The WS<sub>2</sub>-carbon composite powders had better electrochemical properties than the bare WS<sub>2</sub> powders.

## Methods

**Material fabrication.** Spherical WO<sub>3</sub>-carbon and WO<sub>3</sub> powders were prepared directly by spray pyrolysis from spray solutions of ammonium metatungstate with and without a sucrose additive, respectively. The spray pyrolysis system consisted of a droplet generator, a quartz reactor, and a powder collector. The length and diameter of the quartz reactor were 1000 and 55 mm, respectively. A 1.7 MHz ultrasonic spray generator with six vibrators was used to generate a large quantity of droplets, which were carried into the high-temperature tubular reactor by the carrier gas (nitrogen) at a flow rate of 10 L min<sup>-1</sup>. The reactor temperature was fixed at 900°C. The concentrations of the ammonium metatungstate and sucrose were 0.2 and 0.1 M, respectively. The as-prepared WO<sub>3</sub>-carbon and WO<sub>3</sub> powders were converted to WS<sub>2</sub>-carbon and WS<sub>2</sub>, respectively, by adopting a sulfidation process under a reducing atmosphere with thiourea as the sulfur source. The as-prepared powders were placed in a small alumina boat, which was located inside a larger alumina boat. Thiourea was loaded outside of the small alumina boat in excess to form the WS<sub>2</sub>. The sulfidation process was performed at 400°C for 6 h in the presence of a 10% H<sub>2</sub>/Ar mixture gas.

**Characterization.** The crystal structures of the WS<sub>2</sub>-carbon and WS<sub>2</sub> powders were investigated by performing X-ray diffractometry (XRD, Rigaku DMAX-33) using Cu K $\alpha$  radiation at the Korea Basic Science Institute (Daegu). The morphologies of the powders were characterized using scanning electron microscopy (SEM, JEOL JSM-6060) and high-resolution transmission electron microscopy (TEM, JEOL JEM-

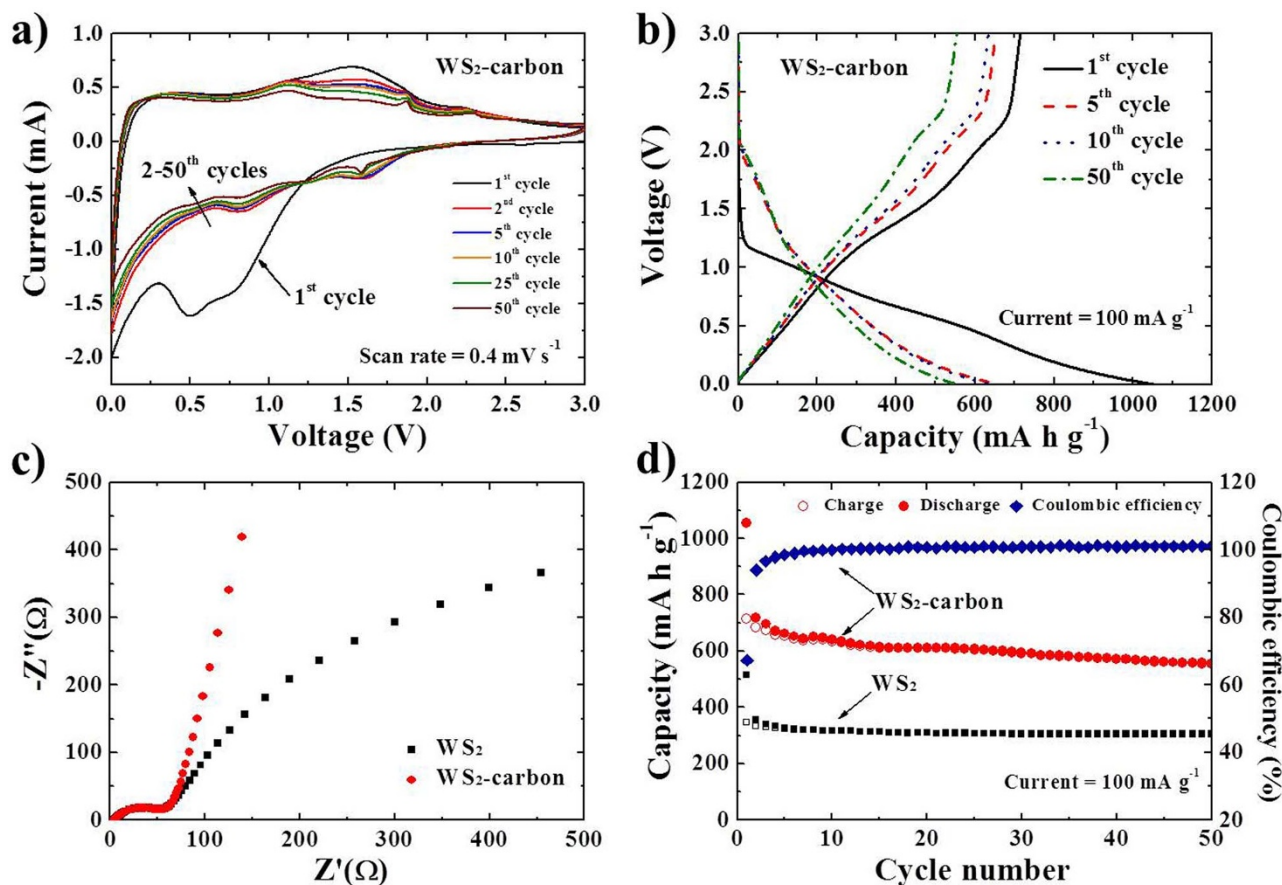


**Figure 5** | Electrochemical properties of the bare WS<sub>2</sub> and WS<sub>2</sub>-carbon composite: a) CV curves of the WS<sub>2</sub>-carbon composite, (b) Cycle profiles of the WS<sub>2</sub>-carbon composite at a current density of 100 mA g<sup>-1</sup>, (c) Nyquist impedance plots before cycling, and (d) Cycle performances at a current density of 100 mA g<sup>-1</sup>.

2010). The specific surface areas of the bare WS<sub>2</sub> and WS<sub>2</sub>-carbon composite powders were calculated by Brunauer-Emmett-Teller (BET) analysis of nitrogen-adsorption measurements (Micromeritics TriStar 3000).

**Electrochemical measurements.** The electrochemical properties of the WS<sub>2</sub>-carbon and WS<sub>2</sub> powders were measured using 2032-type coin cells. The electrodes were prepared by mixing 35 mg of the active powders, 10 mg of carbon black (Super P) as a conductive material, 5 mg of sodium carboxymethyl cellulose (CMC) using distilled water. Lithium metal and a microporous polypropylene film were used as the counter electrode and separator, respectively. LiPF<sub>6</sub> (1 M) in a mixture of ethylene carbonate (EC) and dimethyl carbonate (DMC) in a 1:1 volume ratio with 5 wt% fluoroethylene carbonate (FEC) was used as the electrolyte (Techno Semichem Co.). The entire cell was assembled under an argon atmosphere in a glove box. The charge/discharge characteristics and electrochemical impedance spectroscopy (EIS) measurements of the samples were measured at 100 mA g<sup>-1</sup> in the voltage range of 0.001–3 V. Cyclic voltammetry (CV) measurements were carried out at a scan rate of 0.4 mV s<sup>-1</sup>.

- Lai, C. H., Lu, M. Y. & Chen, L. J. Metal sulfide nanostructures: synthesis, properties and applications in energy conversion and storage. *J. Mater. Chem.* **22**, 19–30 (2012).
- Gao, M. R., Xu, Y. F., Jiang, J. & Yu, S. H. Nanostructured metal chalcogenides: synthesis, modification, and applications in energy conversion and storage devices. *Chem. Soc. Rev.* **42**, 2986–3017 (2013).
- Chhowalla, M. *et al.* The chemistry of two-dimensional layered transition metal dichalcogenide nanosheets. *Nat. Chem.* **5**, 263–275 (2013).
- Wang, Q. H. *et al.* Electronics and optoelectronics of two-dimensional transition metal dichalcogenides. *Nat. Nanotechnol.* **7**, 699–712 (2012).
- Xiao, J. *et al.* Exfoliated MoS<sub>2</sub> nanocomposite as an anode material for lithium ion batteries. *Chem. Mater.* **22**, 4522–4524 (2010).
- Sun, P., Zhang, W., Hu, X., Yuan, L. & Huang, Y. Synthesis of hierarchical MoS<sub>2</sub> and its electrochemical performance as an anode material for lithium-ion batteries. *J. Mater. Chem. A* **2**, 3498–3504 (2014).
- Zhu, C. *et al.* Single-Layered ultrasmall nanoplates of MoS<sub>2</sub> embedded in carbon nanofibers with excellent electrochemical performance for lithium and sodium Storage. *Angew. Chem. Int. Ed.* **53**, 2152–2156 (2014).

- Chang, K. *et al.* Graphene-like MoS<sub>2</sub>/amorphous carbon composites with high capacity and excellent stability as anode materials for lithium ion batteries. *J. Mater. Chem.* **21**, 6251–6257 (2011).
- Shi, Y. *et al.* Self-assembly of hierarchical MoS<sub>2</sub>/CNT nanocomposites (2 < x < 3): towards high performance anode materials for lithium ion batteries. *Sci. Rep.* **3**, 2169 (2013).
- Pham, V. H. *et al.* Liquid phase co-exfoliated MoS<sub>2</sub>-graphene composites as anode materials for lithium ion batteries. *J. Power Sources* **244**, 280–286 (2013).
- Chang, K. *et al.* Ultrathin MoS<sub>2</sub>/nitrogen-doped graphene nanosheets with highly reversible lithium storage. *Adv. Energy Mater.* **3**, 839–844 (2013).
- Wang, Z. *et al.* CTAB-assisted synthesis of single-layer MoS<sub>2</sub>-graphene composites as anode materials of Li-ion batteries. *J. Mater. Chem. A* **1**, 2202–2210 (2013).
- Zhou, X., Wan, L. J. & Guo, Y. G. Synthesis of MoS<sub>2</sub> nanosheet-graphene nanosheet hybrid materials for stable lithium storage. *Chem. Commun.* **49**, 1838–1840 (2013).
- Liu, H., Su, D., Wang, G. & Qiao, S. Z. An ordered mesoporous WS<sub>2</sub> anode material with superior electrochemical performance for lithium ion batteries. *J. Mater. Chem.* **22**, 17437–17440 (2012).
- Shiva, K. *et al.* Employing synergistic interactions between few-layer WS<sub>2</sub> and reduced graphene oxide to improve lithium storage, cyclability and rate capability of Li-ion batteries. *Nano Energy* **2**, 787–793 (2013).
- Bhandavat, R., David, L. & Singh, G. Synthesis of surface-functionalized WS<sub>2</sub> nanosheets and performance as Li-ion battery anodes. *J. Phys. Chem. Lett.* **3**, 1523–1530 (2012).
- Chen, D. *et al.* In situ nitrogenated graphene-few-layer WS<sub>2</sub> composites for fast and reversible Li<sup>+</sup> storage. *Nanoscale* **5**, 7890–7896 (2013).
- Wang, S. *et al.* Synthesis and characterization of cobalt-doped WS<sub>2</sub> nanorods for lithium battery applications. *Nanoscale Res. Lett.* **5**, 1301–1306 (2010).
- Wang, G. X. *et al.* Tungsten disulfide nanotubes for lithium storage. *Electrochem. Solid-State Lett.* **7**, A321–A323 (2004).
- Choi, S. H. & Kang, Y. C. Synthesis for yolk-shell-structured metal sulfide powders with excellent electrochemical performances for lithium-ion batteries. *Small* **10**, 474–478 (2014).
- Ko, Y. N., Choi, S. H., Park, S. B. & Kang, Y. C. Preparation of yolk-shell and filled Co<sub>9</sub>S<sub>8</sub> microspheres and comparison of their electrochemical properties. *Chem. Asian J.* **9**, 572–576 (2014).



22. Shi, Y. *et al.* Hollow structured  $\text{Li}_3\text{VO}_4$  wrapped with graphene nanosheets in situ prepared by a one-pot template-free method as an anode for lithium-ion batteries. *Nano Lett.* **13**, 4715–4720 (2013).
23. Ko, Y. N., Park, S. B., Jung, K. Y. & Kang, Y. C. One-pot facile synthesis of ant-cave-structured metal oxide–carbon microballs by continuous process for use as anode materials in li-ion batteries. *Nano Lett.* **13**, 5462–5466 (2013).

## Acknowledgments

This work was supported by the National Research Foundation of Korea (NRF) grant funded by the Korea government (MEST) (No. 2012R1A2A2A02046367). This work was supported by the Energy Efficiency & Resources Core Technology Program of the Korea Institute of Energy Technology Evaluation and Planning (KETEP), granted financial resource from the Ministry of Trade, Industry & Energy, Republic of Korea (201320200000420).

## Author contributions

S.H.C., J.H.L. and Y.C.K. devised the concept, designed the experiment, and wrote the manuscript. S.H.C. and S.J.B. performed the experiments and analyzed the data. Y.C.K. supervised the project. All authors discussed the results and contributed in this manuscript.

## Additional information

**Supplementary information** accompanies this paper at <http://www.nature.com/scientificreports>

**Competing financial interests:** The authors declare no competing financial interests.

**How to cite this article:** Choi, S.H., Boo, S.J., Lee, J.-H. & Kang, Y.C. Electrochemical properties of tungsten sulfide–carbon composite microspheres prepared by spray pyrolysis. *Sci. Rep.* **4**, 5755; DOI:10.1038/srep05755 (2014).



This work is licensed under a Creative Commons Attribution-NonCommercial-ShareAlike 4.0 International License. The images or other third party material in this article are included in the article's Creative Commons license, unless indicated otherwise in the credit line; if the material is not included under the Creative Commons license, users will need to obtain permission from the license holder in order to reproduce the material. To view a copy of this license, visit <http://creativecommons.org/licenses/by-nc-sa/4.0/>